Appendix A

Atomic Units

The atomic unit system is based on the following definitions:

$$\bar{h} = m_e = e = 4\pi\varepsilon_0 = 1, \tag{A.1}$$

where $\bar{h}$ is Plancks constant divided by 2π, m_e and $-e$ are the mass and the charge of the electron, respectively, and ε_0 the permittivity of free space. From the dimensionless fine structure constant $\alpha = e^2/4\pi\varepsilon_0 c = 1/137$ one directly sees that the speed of light c in this unit system has a numerical value of 137.

With these definitions all physical quantities are related to that of the hydrogen atom, giving a natural scale in atomic physics. As an example, the Bohr radius a_0, being the radius of the electron in the hydrogen ground state in Bohr's atomic model, is given by $a_0 = 4\pi\varepsilon_0\bar{h}^2/m_e e^2 = 1$. An overview of the most important quantities is given in table A.1. One important note is that 1 atomic unit of energy does not correspond with the binding energy of the ground state hydrogen atom of 13.6 eV, but to its potential energy of 27.2 eV.

Throughout this thesis both the projectile velocity and kinetic energy are used. For non-

Quantity	SI value	non-SI value	definition
length	$5.29177249 \times 10^{-11}$ m	0.529 Å	a_0
time	$2.41888433 \times 10^{-17}$ s		$a_0(\alpha c)^{-1}$
velocity	2.18769142×10^{6} m/s		αc
mass	$9.1093897 \times 10^{-31}$ kg	511 keV/c^2	m_e
energy	4.3593×10^{-18} J	27.2 eV	$m_e(\alpha c)^2$
charge	$1.6021773 \times 10^{-19}$ C		e
momentum	$1.99285337 \times 10^{-24}$ kgm/s		$m_e \alpha c$
angular momentum	$1.0545887 \times 10^{-34}$ Js		$\bar{h} = m_e \alpha c a_0$

Table A.1: *Overview of the most important physical quantities, giving the SI values related to 1 atomic unit of the corresponding quantity.*

relativistic collision energies the relation between them is given by:

$$\mathrm{v}_p(\text{a.u.}) = 0.20\sqrt{E\,(\text{keV/amu})}, \tag{A.2}$$

where the projectile energy E is in keV/amu and the projectile velocity v_p in atomic units. Note that 1 atomic mass unit (amu) is 1/12 of the mass ^{12}C, which is different from one unit of mass in atomic units.

The obtained quantities related to the recoil experiments in this thesis are frequently given in units of momentum. For Na 1 a.u. of momentum corresponds to a velocity of 52 m/s or a kinetic energy of 0.3 meV. The longitudinal momenta p_{long} in atomic units are transformed into Q-values, given in eV, via:

$$Q(\text{eV}) = 27.2\mathrm{v}_p(\text{a.u.})\left[p_{long}(\text{a.u.}) + 0.5r\mathrm{v}_p(\text{a.u.})\right], \tag{A.3}$$

where v_p(a.u.) is the projectile velocity in atomic units and r is the number of transferred electrons. The relation between the scattering angle and the transverse momentum p_{trans} in atomic units is:

$$\theta(\text{rad}) = \frac{p_{trans}(\text{a.u.})}{1836M(\text{amu})\mathrm{v}_p(\text{a.u.})}. \tag{A.4}$$

Appendix B

Numerical Abel Transformation

The transverse momentum distributions $\sigma(p_{trans})$ or differential cross sections $\sigma(\theta)$ and the experimentally obtained $p_{trans,y}$ or θ_y distributions are connected by the so-called inverse Abel transformation [152]. In short, due to the cylindrical symmetry around the projectile axis (x-axis), the scattering pattern only depends on scattering angle θ, i.e. $I(\phi,\theta) = I(\theta) = C\sigma(\theta)$, where C is some constant and angles ϕ and θ are related to the recoil momentum components $p_{trans,y}$ and $p_{trans,z}$ through

$$\phi = -\tan\left(\frac{p_{trans,y}}{p_{trans,z}}\right), \tag{B.1}$$

$$\theta = \frac{p_{trans}}{m_p \mathrm{v}_p} = \frac{1}{m_p \mathrm{v}_p}\sqrt{p_{trans,y}^2 + p_{trans,z}^2}, \tag{B.2}$$

where m_p and v_p are the mass and velocity of the projectile, respectively (see also figure 4.18 for the experimental geometry). The measured 1D scattering pattern $I_j(\theta_j) = I_j(p_{trans,j}/(m_p \mathrm{v}_p))$ ($j = y,z$) is an effective projectile of the 2D scattering pattern $I(\theta)$ onto the y or z axis and are related via:

$$I_j(\theta_j) = 2\int_{\theta_j}^{\infty} \frac{I(\theta)\theta \mathrm{d}\theta}{\sqrt{\theta^2 - \theta_j^2}} \equiv \mathscr{A}[I(\theta)], \tag{B.3}$$

where $\mathscr{A}$ is the Abel transformation. Thus by inverting this transformation the scattering pattern $I(\theta)$ can be extracted from only one component $I_j(\theta_j)$:

$$I(\theta) = \mathscr{A}^{-1}[I_j(\theta_j)] = -\frac{1}{\pi}\int_{\theta}^{\infty} \frac{\mathrm{d}I_j/\mathrm{d}\theta_j}{\sqrt{\theta_j^2 - \theta^2}} \mathrm{d}\theta_j, \tag{B.4}$$

where $\mathscr{A}^{-1}$ is the inverse Abel transformation. This relation enables us to obtain the differential cross section or transverse momentum distribution from the distribution of $p_{trans,y}$ only.

Directly applying the inverse Abel transformation turns out to be quite sensitive to statistical noise because it involves the derivative of the measured distribution. To overcome this

problem a new method for performing the inverse Abel transformation has been developed, especially designed to deal with noisy data[1]. Our approach is based on an earlier iterative procedure of Vrakking [170]. We have extended this method by including additional smoothing and weighting conditions in the iteration formula in order to achieve better convergence and a smoother final result. This method allows us to extract valuable information also for data points close to the origin, where usually the noise of the transformation is accumulated. We apply our method to the inversion of one-dimensional problems and compare it to the standard inverse Abel transformation.

We start with introducing the iterative method of Vrakking, which was designed to extract the three dimensional velocity distribution of two dimensional images in ion or photoelectron imaging experiments. In brief, the rotationally symmetric 3D velocity distribution $P(\mathrm{v},\theta)$ is rewritten as a product of two distributions, of which one only depends on the velocity [2]:

$$P(\mathrm{v},\theta) = P_1(\mathrm{v})P_2(\mathrm{v},\theta). \tag{B.5}$$

The same ansatz is made for the measured 2D projection on the detector:

$$Q_{\mathrm{exp}}(\mathrm{v},\alpha) = Q_{1,\mathrm{exp}}(\mathrm{v})Q_{2,\mathrm{exp}}(\mathrm{v},\alpha). \tag{B.6}$$

Here, $Q_{\mathrm{exp}}(\mathrm{v},\alpha)$ is the measured 2D image. The relation between the position on the detector R and the initial velocity v is given by $R = \mathrm{v}t$, where t is the time of flight to the detector. The subsequent functions that appear during the iteration procedure are labelled with $P_{1,i}$, $P_{2,i}$, $Q_{1,i}$ and $Q_{2,i}$, and the starting values are given by

$$P_{1,i=0}(\mathrm{v}) = Q_{1,\mathrm{exp}}(R)/(2\pi R) \tag{B.7}$$

$$P_{2,i=0}(\mathrm{v},\theta) = Q_{2,\mathrm{exp}}(R,\alpha=\theta). \tag{B.8}$$

The iteration procedure goes as follows: given the function $P_{1/2,i}$ the 2D projections $Q_{1/2,i}$ are calculated. Then the next iteration $P_{1/2,i+1}$ is determined according to the following two equations:

$$P_{1,i+1}(\mathrm{v}) = P_{1,i}(v) - c_1\frac{Q_{1,i}(R) - Q_{1,\mathrm{exp}}(R)}{2\pi R} \tag{B.9}$$

$$P_{2,i+1}(\mathrm{v},\theta) = P_{2,i}(v,\theta) - c_2\left[(Q_{2,i}(R,\alpha=\theta) - Q_{2,\mathrm{exp}}(R,\alpha=\theta)\right]. \tag{B.10}$$

These equations lie at the heart of the iteration. Apart from the origin, these procedure gives reliable results and a good reconstruction of the 3D distribution. For a more detailed outline of the procedure we refer to the original paper of Vrakking [170].

In the special case of a rotationally symmetric 2D distribution that is projected onto a single line, the above procedure is much simpler because both distributions depend only on the radial velocity. Therefore we can write:

$$P_{2\mathrm{D}}(\mathrm{v}) \tag{B.11}$$

$$Q_{\mathrm{exp}}(\mathrm{v}) \tag{B.12}$$

[1] This method is developed and discussed by Herwig Ott [169], from which a shortened version is given here.

[2] Functions and distributions that are defined in real space are labelled with p or P, whereas the projected functions and distributions in the imaging plane are labelled with q and Q. We refer to these two "spaces" also "P-space" and "Q-space".

for the original 2D distribution $P(\mathrm{v})$ and the measured line distribution $Q_{\mathrm{exp}}(\mathrm{v})$. Again, the position on the detector is converted into a velocity via the time of flight condition $R = \mathrm{v}t$, where t is the time of flight. The starting value for the 2D distribution is

$$P_0(\mathrm{v}) = Q_{\mathrm{exp}}(\mathrm{v})/(2\pi\mathrm{v}). \tag{B.13}$$

The initial distribution is not a crucial quantity because the functions rapidly converge to the real distribution. For simplicity we can also set

$$P_0(\mathrm{v}) = Q_{\mathrm{exp}}(\mathrm{v}) \tag{B.14}$$

as initial condition. The iteration procedure now looks much simpler:

$$P_{i+1}(\mathrm{v}) = P_i(\mathrm{v}) - c_1 \frac{Q_i(\mathrm{v}) - Q_{\mathrm{exp}}(\mathrm{v})}{2\pi\mathrm{v}} \tag{B.15}$$

$$Q_{i+1}(\mathrm{v}) = 2\int_{\mathrm{v}}^{\infty} P_{i+1}(\mathrm{v}') \frac{\mathrm{v}'}{\sqrt{\mathrm{v}'^2 - \mathrm{v}^2}} d\mathrm{v}', \tag{B.16}$$

where the latter is the Abel transformation of $P_{i+1}(\mathrm{v})$ to get the new projection $Q_{i+1}(\mathrm{v})$.

Before we present our modification to this treatment, we introduce the discretization of the problem. Due to the finite pixel size of the detector, the data come as a list of data points (labelled with j)

$$Q_i(\mathrm{v}) := Q_{ij}(\mathrm{v}_j). \tag{B.17}$$

Accordingly, the discrete versions of the equations (B.14-B.16) are

$$P_{0j}(\mathrm{v}_j) = Q_{\mathrm{exp},j}(\mathrm{v}_j) \tag{B.18}$$

$$P_{i+1,j}(\mathrm{v}_j) = P_{ij}(\mathrm{v}_j) - c_1 \frac{Q_{ij}(\mathrm{v}_j) - Q_{\mathrm{exp},j}(\mathrm{v}_j)}{2\pi\mathrm{v}_j} \tag{B.19}$$

$$Q_{i+1,j}(\mathrm{v}_j) = 2\sum_{k=j+1}^{j_{\max}} P_{i+1,k}(\mathrm{v}_k) \frac{\mathrm{v}_k}{\sqrt{\mathrm{v}_k^2 - \mathrm{v}_j^2}} (\mathrm{v}_k - \mathrm{v}_{k-1}). \tag{B.20}$$

Here, $j_{\max}$ is the highest entry for the data and $\mathrm{v}_k - \mathrm{v}_{k-1} = \Delta\mathrm{v}_k$ is the step size between two neighboring data points, which in general will be independent of k, so that we can replace it with $\Delta\mathrm{v}$. To avoid a division by zero, the sum starts with $j+1$.

In our modified version of the iteration, we add an additional term to the iteration equation B.19:

$$P_{i+1,j}(\mathrm{v}_j) = P_{ij}(\mathrm{v}_j) - c_1 \frac{Q_{ij}(\mathrm{v}_j) - Q_{\mathrm{exp},j}(\mathrm{v}_j)}{2\pi\mathrm{v}_j} - c_2 \left(P_{ij}(\mathrm{v}_j) - \frac{1}{2}\left[P_{i,j-1}(\mathrm{v}_j) + P_{i,j+1}(\mathrm{v}_j)\right] \right). \tag{B.21}$$

The new correction term with weight c_2 is a correction in "P-space", where any data point of P_i is compared with the two neighboring ones. If it is not the arithmetic average the new calculated data point gets a correction towards to arithmetic average. This procedure tries to smoothen the P_i functions. On the other hand, this smoothing is balanced by the first correction factor, which tries to change the P_i function in order to perfectly describe the data. Without the smoothing algorithm, the c_1 term tends to generated large noise for a high number of iterations and the final result hardly converges.

Appendix C

Extraction of Ionization Events in Non-Coincident Recoil Spectra

The experiments described in this thesis are based on recoil-ion momentum spectroscopy in which only the recoil target ions have been measured. For pure (multi-)electron capture processes, the momenta of the recoil ions contain the full kinematics. For processes in which one or more electrons are emitted to the continuum, i.e., (multiple) ionization, a measurement the momenta of the recoil and all free electrons is necessary to obtain the complete information. However, the recoil experiments which do not detect the emitted electron and the charge-changed projectile, still reveals a part of the ionization information. Here we will show that in our Q-value spectra ionization processes can be separated from those of capture and by this cross sections for ionization can be obtained.

Let us consider the case of singly charged recoils, which can be produced by either one-electron capture or single ionization. For one-electron capture the relation between the longitudinal momentum of the recoil ion and the Q-value is given by:

$$p_{long} = \frac{Q}{\mathrm{v}_p} - \frac{1}{2}\mathrm{v}_p \tag{C.1}$$

with Q the difference between the total binding energies before and after the reaction, and v_p the projectile velocity. For single ionization the longitudinal momentum is given by:

$$p_{long} = \frac{I + E_e}{\mathrm{v}_p} - p_{e,long} \tag{C.2}$$

with E_e the kinetic energy and $p_{e,long}$ the longitudinal momentum of the emitted electron. We are applying equation C.1 to the measured longitudinal momenta of the singly charged recoils to obtain the Q-value spectra. Question is at which Q-values the ionization events appear and whether they will interfere with the capture events.

To do so we have to connect equation C.1 and C.2. First we write the properties of the

emitted electron in terms of the projectile velocity:

$$p_{e,long} = \alpha \mathrm{v}_p, \tag{C.3}$$

$$p_{e,trans} = \beta \mathrm{v}_p, \tag{C.4}$$

$$E_e = \frac{1}{2}(\alpha^2+\beta^2)\mathrm{v}_p^2, \tag{C.5}$$

where α and β can yield positive and negative values. If we plug equations C.3-C.5 into equation C.2 and equate this to equation C.1 one finds the following relation between Q, I and the properties of the emitted electron:

$$Q = I + \frac{1}{2}\left[(\alpha-1)^2+\beta^2\right]\mathrm{v}_p^2. \tag{C.6}$$

Defining the following quantity:

$$\eta \equiv (\alpha-1)^2+\beta^2 \tag{C.7}$$

leads to the following simple equation:

$$Q = I + \frac{1}{2}\eta \mathrm{v}_p^2 \tag{C.8}$$

Because $\eta \geq 0$ in all cases $Q \geq I$ and therefore ionization events will always appear at the right side of the ionization limit in the recoil spectrum. Thus $Q = I$ acts as a marker in the Q-value spectrum, separating the capture and ionization contributions. A sharp onset of ionization at $Q = I$ has indeed been observed experimentally in singly charged recoil spectra which are taken in coincidence with the emitted electron [175].

After further inspection of equations C.7 and C.8, one recognizes that $\frac{1}{2}\eta\mathrm{v}_p^2$ is simply the electron kinetic energy in the projectile frame. One might even extract more information about the emitted electron, based the Q-value spectra part of $Q \geq I$. Experiments on slow ion-atom collisions measuring the recoil momentum of the emitted electron found that the electron travels mainly along the projectile axis, thus having small transverse momentum. Furthermore, that electron is mainly found at the target or the projectile or in between and much less intensity is found for electron moving backwards or accelerated to the higher velocity than the projectile (see e.g. [123–125]). Therefore we make the assumption that $\beta = 0$ and consider only the cases the $0 \leq \alpha \leq 1$.

Firstly, $\alpha = 1$ means $\eta = 0$ and the electron has no kinetic energy in the projectile frame, thus moving along with the projectile. This corresponds to the process of electron capture into the continuum (ECC). These events contribute the recoil spectra at the boundary $Q = I$. ECC can be seen as a smooth continuation of capture into high n-states, in the limit $n \to \infty$. Secondly, $\alpha = 0$ or $\eta = 1$ corresponds to the situation that the emitted electron has zero energy in the target frame, i.e. it stays near the target recoil. This results in the maximum kinetic energy in the projectile frame and contributes at $Q = I + \frac{1}{2}\mathrm{v}_p^2$. This process is called electron excitation to the continuum (EEC). For all other cases $0 < \eta < 1$ holds and the emitted electron is found in between the projectile and the target, contributing to the region between I and $I + \frac{1}{2}\mathrm{v}_p^2$ in the Q-value spectrum.

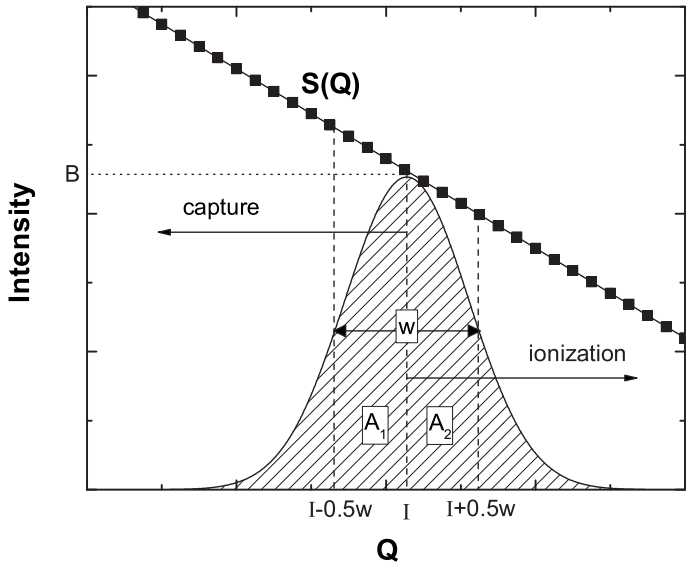

Figure C.1: *Schematic representation of the Q-value spectra around the boundary between capture and ionization. Using a Gaussian distribution at $Q = I$ with a FWHM equal to the Q-value resolution one can estimate the amount of capture events appearing at $Q > I$ and ionization events at $Q < I$ and correct for this.*

Here only the case of singly charged recoils has been shown in detail, but this derivation can be extended to multiple charged recoil ions. For instance doubly charged recoil can be created in three way: double electron capture, transfer ionization (one-electron capture accompanied with single ionization) and double ionization. These processes can be separated in the same manner as described above. However, here the analysis is slightly less straight forward than for singly charged recoil ions. For example, two electron can be captured in a projectile state which lies above the first ionization potential. Nevertheless, in practise this does not have to lead to ambiguities as long these excited states lie well above the ionization potential. As has been shown for the Na^{2+} recoils in He^{2+}+Na collisions, transfer ionization to He^{+}(n=1) do not overlap with double capture to He(n=2,n'), and double capture and transfer ionization can be separated (see figure 6.11).

Although the ionization potentials represents sharp boundaries, due to the finite experimental resolution capture events can appear at $Q > I$ and ionization events at $Q < I$. To correct for this effect we have applied the following procedure, which is illustrated by figure C.1. In 0'th order, without correction, one can take the area of spectrum $S(Q)$ for $Q < I$ as the total capture σ^0_{cap} and the area for $Q > I$ as the total ionization cross section σ^0_{ion}, i.e.,

$$\sigma^0_{\mathrm{cap}} = \int_{-\infty}^{I} S(Q)\mathrm{d}Q, \tag{C.9}$$

$$\sigma^0_{\mathrm{ion}} = \int_{I}^{\infty} S(Q)\mathrm{d}Q. \tag{C.10}$$

The influence of the experimental resolution can be estimated by taking a Gaussian distribution with a full width half maximum (FWHM) of w, equal to the Q-value resolution. The area underneath this curve represents the amount of events which origin has to reconsidered. This area A can be easily determined from $S(Q)$, namely $A = Bw\sqrt{\pi/2}$, where $B = S(I)$. The balance between capture and ionization events appearing on the "wrong" side of $Q = I$ depends on the shape of $S(Q)$. For example, for an decreasing behavior of $S(Q)$ (as depicted in figure C.1) the capture cross section is underestimated while the ionization cross section is overestimated in 0'th order and the amount depends on the steepness of $S(Q)$.

To take this into account we compare the areas underneath the spectrum directly before and after $Q = I$,

$$A_1 = \int_{I-\frac{1}{2}w}^{I} S(Q)\mathrm{d}Q, \tag{C.11}$$

$$A_2 = \int_{I}^{I+\frac{1}{2}w} S(Q)\mathrm{d}Q, \tag{C.12}$$

where the boundaries are taken at $Q = I \pm \frac{1}{2}w$. This is a rather arbitrary choice but facilitates a consistent treatment of spectra with different resolutions. The relative size of these areas gives the amount of A with which the 0'th order cross sections have to corrected, finally leading to:

$$\sigma_{\mathrm{cap}} = \sigma^0_{\mathrm{cap}} + \left(\frac{A_1}{A_1+A_2} - \frac{1}{2}\right) A = \sigma^0_{\mathrm{cap}} + \frac{1}{2}\frac{A_1-A_2}{A_1+A_2}A, \tag{C.13}$$

$$\sigma_{\mathrm{ion}} = \sigma^0_{\mathrm{ion}} + \left(\frac{A_2}{A_1+A_2} - \frac{1}{2}\right) A = \sigma^0_{\mathrm{ion}} + \frac{1}{2}\frac{A_2-A_1}{A_1+A_2}A. \tag{C.14}$$

where one has to take in mind that in the 0'th order one already assigns an area of $\frac{1}{2}A$ to both cross sections. In this way the events in the neighborhood of the ionization potential boundary are redistribution over the capture and ionization cross sections.

Appendix D

Alignment and orientation properties of Na$^*(3p)$ in a MOT

Collision experiments with excited target atoms are often performed to study the dependence of the cross section on the alignment or orientation of the target with respect to the projectile axis. This requires the experimental control over the population of the magnetic substates, which is e.g. possible by means of laser excitation [255, 256].

For excited Na$^*(3p)$ the electronic state can in general be represented by a linear superposition of the m-substates:

$$|3p\rangle = a_0|3p_0\rangle + a_{+1}|3p_{+1}\rangle + a_{-1}|3p_{-1}\rangle. \tag{D.1}$$

An oriented $3p$ state results from an asymmetric population of the m quantum number around $m = 0$, i.e. $a_{+1} \neq a_{-1}$, which can be obtained experimentally by optical pumping with circularly polarized light [282]. A pure oriented state has either an m-distribution according to $a_{+1} = 1$, $a_0 = a_{-1} = 0$ or $a_{-1} = 1$, $a_0 = a_{+1} = 0$. The resulting electron cloud is ring shaped with a clockwise or counter-clockwise intrinsic motion.

For the theoretical treatment of collision processes it is often more convenient to consider basis states with well defined (reflection) symmetry with respect to the scattering plane. Instead of using m-substates one often uses pure atomic states to describe the collision processes,

$$\begin{aligned} |\sigma\rangle &= |p_0\rangle, \\ |\pi^+\rangle &= -\frac{1}{\sqrt{2}}(|p_{+1}\rangle - |p_{-1}\rangle), \\ |\pi^-\rangle &= \frac{i}{\sqrt{2}}(|p_{+1}\rangle - |p_{-1}\rangle), \end{aligned} \tag{D.2}$$

whereby + and - indicate positive or negative reflection symmetry of the wavefunction with respect to the scattering plane. In this basis the Na$(3p)$ state can be written as:

$$|3p\rangle = a_\sigma|3p\sigma\rangle + a_{\pi^+}|3p\pi^+\rangle + a_{\pi^-}|3p\pi^-\rangle, \tag{D.3}$$

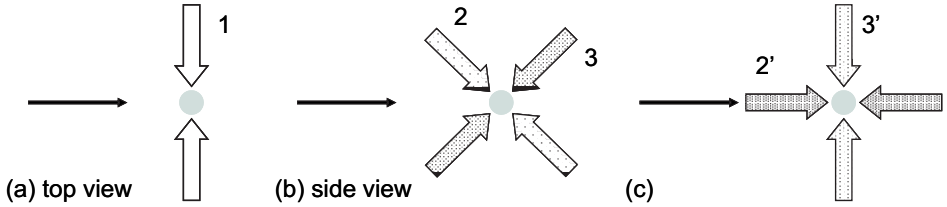

Figure D.1: *Schematic representation of the MOT laser beams with respect to the ion beam (⟶): (a) top view, showing the horizontal beam pair 1, which is perpendicular to the ion beam, (b) side view, showing diagonal beam pairs 2 and 3, which cross the ion beam under approximately 45°. Laser beams 2 and 3 can be decomposed into laser beams 2' and 3', which are parallel and perpendicular to the ion beam, respectively, as shown in (c).*

in which the amplitudes are transformed as follows:

$$\begin{aligned} a_\sigma &= a_0, \\ a_{\pi^+} &= -\frac{1}{\sqrt{2}}(a_{+1} - a_{-1}), \\ a_{\pi^-} &= -\frac{i}{\sqrt{2}}(a_{+1} + a_{-1}). \end{aligned} \tag{D.4}$$

These atomic orbitals have a "dumb-bell" shape, either parallel (σ) or perpendicular ($\pi^{+/-}$) to the ion beam axis. Therefore it is a natural choice to use the atomic states for describing collisions involving aligned Na*($3p$). Alignment is connected to an equal population of the $|m|$-states, i.e. $|a_{+1}| = |a_{-1}|$. Explicitly, for a pure aligned $|3p\sigma\rangle$ state $a_0 = 1$ and $a_{+1} = a_{-1} = 0$, $|3p\pi^+\rangle$ results from $a_0 = 0$ and $a_{+1} = -a_{-1}$ and finally $|3p\pi^-\rangle$ is connected to $a_0 = 0$ and $a_{+1} = a_{-1}$. Experimentally these states can be obtained by optical pumping with linearly polarized light [282]. Experiments in which the collision plane is not defined do not allow measurements on $|3p\pi^+\rangle$ and $|3p\pi^-\rangle$ separately. In these cases one obtains the average over these states, which is called $|3p\pi\rangle$.

For collisions measurements on aligned target atoms the measured cross sections $\sigma_\parallel$ and $\sigma_\perp$ for laser polarization perpendicular and parallel to the ion beam, respectively, are connected to the σ_σ and σ_π cross sections for capture from "pure" prepared σ or π atomic orbitals via [200, 282]

$$\sigma_\parallel = (5\sigma_\sigma + 4\sigma_\pi)/9, \tag{D.5}$$

$$\sigma_\perp = (2\sigma_\sigma + 7\sigma_\pi)/9. \tag{D.6}$$

To connect the situation of a single linearly polarized laser beam with our MOT setup, consisting of six circularly polarized laser beams, the following analysis is given. First of all lets recall that circularly polarized light can be written as a superposition of linearly polarized light. Furthermore, the relative phases of the two components are not of importance here, such that we do not have to distinguish between σ^+ and σ^- polarized light.

In figure D.1 the geometry in the present experiment is depicted for the six laserbeams with respect to the ion beam. Laser beam pair 1, which is in the horizontal plane, is perpendicular to the ion beam, which means that the linear components are both parallel and

perpendicular to the ion beam. Therefore the contribution of laser beam pair 1 to the cross section can be written as

$$\sigma(1) = \frac{1}{2}(\sigma_{\perp} + \sigma_{\parallel}). \tag{D.7}$$

The other laser beams are diagonally placed and therefore cross the ion beam under approximately 45°. However, laser beam pairs 2 and 3 can be decomposed in components either parallel or perpendicular to the ion beam, resulting in pairs 2' and 3'. In fact, because the only constraint in the MOT configuration is the orthogonality of the 3 pairs of laser beams, pairs 2 and 3 can be rotated under an arbitrary angle in the plane defined by themselves. Concerning pair 3' the same argument can be used as for pair 1, leading to

$$\sigma(3') = \frac{1}{2}(\sigma_{\perp} + \sigma_{\parallel}). \tag{D.8}$$

However, pair 2' is parallel to the ion beam, which means that both the linear components are perpendicular to the ion beam. Therefore its contribution to the cross section is given as

$$\sigma(2') = \sigma_{\perp}. \tag{D.9}$$

Because the atoms are excited by all the laser beams in a random way we can add these contributions and fill in equations D.5 and D.6:

$$\sigma_{\mathrm{MOT}} = \frac{1}{3}[\sigma(1) + \sigma(2') + \sigma(3')] = \frac{1}{3}(\sigma_{\parallel} + 2\sigma_{\perp}) = \frac{1}{3}\sigma_{\sigma} + \frac{2}{3}\sigma_{\pi}. \tag{D.10}$$

Thus one can assume a pure unpolarized sample of Na($3p$) atoms in the MOT, in which one can consider equal population for the atomic orbitals σ, π^+ and π^- or equivalently equal population for the m-substates of the Na($3p$) state.